Process Control and Monitoring of Reactive Crystallization of L-Glutamic Acid

Hannu Alatalo, Henry Hatakka, Jarno Kohonen, Satu-pia Reinikainen, and Marjatta Louhi-kultanen
Dept. of Chemical Technology, Lappeenranta University of Technology, FI-53851 Lappeenranta, Finland

DOI 10.1002/aic.12140
Published online December 30, 2009 in Wiley InterScience (www.interscience.wiley.com).

The aim of the present study was to investigate feedback control of a reactive crystallization process. The present study built up a control structure needed to control the driving force of reactive crystallization using the feed rate of added acid. The concentration of the crystallizing compound and pH was used to compute feedback in the closed-loop control of semi-batch precipitation. The concentration of L-glutamic acid was determined from measured MID-IR ATR-FTIR spectra based on a multivariate model. Dynamic change of set value was based on the mass of added sulfuric acid and pH. The studied properties of the product crystals were polymorphism and crystal size. The polymorphic composition was analyzed with a Raman spectrometer and was expressed by mass fraction of the α-polymorph. The obtained results showed that the developed feedback process control system allows effective control of forming of polymorphs. © 2009 American Institute of Chemical Engineers *AIChE J*, 56: 2063–2076, 2010
Keywords: ATR-FTIR, reactive crystallization, closed loop control, process control, L-glutamic acid

Introduction

The desired qualities of a crystalline product are a result of optimization of the chemical composition and process conditions. Results of crystallization studies are needed to improve production economics and to satisfy customers' quality requirements regarding polymorph, crystal size distribution, filterability, crystal habit, and purity.

The development of process analytical technology (PAT) has been intensive during recent years. In the area of crystallization processes, for instance, several studies have been published about spectroscopy-based monitoring and closed loop control of batch cooling crystallization.[1–4] Examples include Nagy et al.[3] who use a set point trajectory of concentration inside the metastable range in cooling crystallization. In their study, dynamic change in set value to produce a constant driving force for kinetic crystallization phenomena is based on temperature-dependent set point trajectory. Kee et al.[5] and Khan et al.[4] base their closed loop control on ATR-FTIR measurements. Kee et al. use supersaturation as a feedback signal to control seeded cooling crystallization in production of α-form L-glutamic acid and Khan et al. use relative supersaturation, c/c^*, to control cooling crystallization of L-glutamic acid to produce a needle-shaped stable β-polymorph. Schöll et al.[6] use pH shift precipitation when studying the nucleation kinetics of L-glutamic acid. Their study of the kinetic nucleation rate is based on ATR-FTIR spectroscopy with pH shift precipitation of glutamic acid from a mono sodium glutamate solution using a HCl reagent.

Abebe et al.[7] have shown that NIR spectra from a transflectance probe (12 mm optical path length) give information about crystal size, crystal concentration, and crystal polymorph at a wave number range of 12,000–5000 cm^{-1}. For supersaturation control purposes, concentration measurement at the MID-IR range, where solids have minor effect on the analysis, is practical despite the risks of mechanical and chemical damage and encrustation of the infrared element (IRE). The geometry of the IRE and the difference in the refractive index between the solution and the IRE affect the penetration depth of the incoming radiation.[8(p. 562)] The IRE material of the ATR probe has to be selected so that the depth of penetration of the infrared energy field into the

Correspondence concerning this article should be addressed to H. Alatalo at hannu.alatalo@lut.fi.

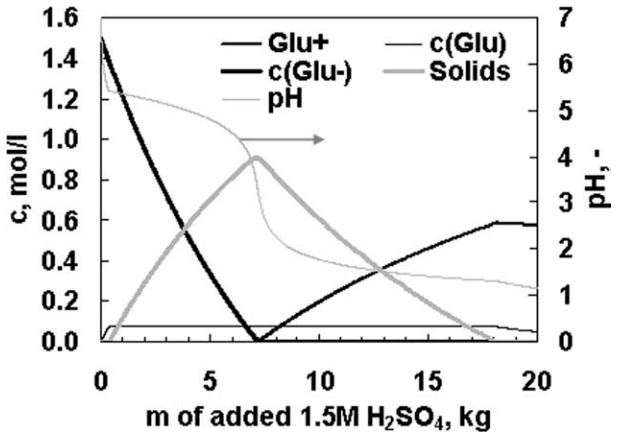

Figure 1. Equilibrium concentrations and pH of 1.5 M mono sodium glutamate with 1.5 M sulfuric acid additions at 25°C.

Initial volume of MSG was 13.4 dm.[3]

solution is smaller than the liquid phase barrier between the probe and the solid crystal particles.[2(p. 89)]

The present study focused on the feasibility of using ATR-FTIR based closed loop control to control crystal quality in a reactive semi-batch crystallization process. L-Glutamic acid was selected as the model compound because process control affects the polymorphic content of the product crystals.[9] L-Glutamic acid is reported to have two polymorphs: a metastable α form and a stable β form.[10] The used concentrations of reagents were in the range where preliminary experiments found that a mixture of polymorphs exists.

Closed-loop process control systems have mostly been developed for batchwise cooling crystallization. To improve reproducibility and uniformity between different batches or campaigns of precipitation processes, it is essential that the process controllability be improved. The present study shows that precipitation processes can be controlled in a sophisticated way with the aid of spectroscopic methods.

Glutamic Acid: Solution and Crystals

L-Glutamic acid (Glu, $C_5H_9NO_4$) and its anion (glutamate, Glu^-, $C_5H_8NO_4^-$), like amino acids in general, are of great importance in biological systems. Examples of L-glutamic acid and glutamate ion reactions are: transamination of L-glutamic acid in amino acid formation of plants,[11(p. 66)] L-glutamine synthesis from L-glutamic acid in nitrogen fixing root nodules of trees,[11(p. 64), 12(p. 288)] the release of the energy of proteins [25% of the body's energy reserve[13(p. 217)]] with transamination and oxidative deamination in the human body (metabolism),[12(p. 295)] about 75% of excitatory neurotransmission in brains,[12(p. 743),14] and as a flavor enhancer (E620 and E621). L-Glutamic acid can be used for example as an admixture in crystallization to improve the separation efficiency of chiral isomers of asparagines.[15] The nucleation rate and growth of glutamic acid can be modified with 1-aspartic acid, 1-valine, 1-leucine, and 1-phenylalanine.[16(p. 250)]

In the present study, glutamic acid is precipitated from a mono sodium glutamate solution by the addition of sulfuric acid in a reactive semi-batch crystallization process. Borissova et al.[17] and Schöll et al.[6] have studied acidification of monosodium glutamate with HCl in semi-batch crystallizers. Borissova et al. have developed a kinetic simulation model for reactive crystallization and have detected the beginning of nucleation with turbidity measurement and the extent of the reaction with pH measurement. The choice of sulfuric acid as a reagent in this study instead of the strong acid, HCl, means that the second equilibrium constant of the dissociation reaction of sulfuric acid has to be taken into account in computation of the reaction equilibrium. The chemical properties of the studied solution are a result of: the acid–base reactions of glutamic acid (Eqs. 1 and 2); the solid–liquid equilibrium (Eq. 3); the acid–base reactions of sulfuric acid (Eqs. 4 and 5); and autoprotolysis of water (Eq. 6). The reaction equilibrium can be solved with electroneutrality (Eq. 7) and mass balance (Eq. 8) equations.

Reactions of glutamic acid[18]:

$$C_5H_{10}NO_4^+(aq) \leftrightarrow C_5H_9NO_4(aq) + H^+(aq) \qquad K_a = 6.2 \times 10^{-3} \quad (1)$$

$$C_5H_9NO_4\ (aq) \leftrightarrow C_5H_8NO_4^-(aq) + H^+(aq) \qquad K_a = 4.57 \times 10^{-5} \quad (2)$$

Solid–liquid equilibrium[6]:

$$C_5H_9NO_4\ (s) \leftrightarrow C_5H_9NO_4(aq) \quad c^*(\beta) = 5.6 \times 10^{-2}\text{mol/L} \qquad c^*(\alpha) = 7.4 \times 10^{-2}\text{mol/L} \quad (3)$$

Reactions of sulfuric acid[19]:

$$H_2SO_4\ (aq) \rightarrow HSO4^-\ (aq) + H^+\ (aq) \quad (4)$$

$$HSO_4^-(aq) \leftrightarrow SO_4^{2-}(aq) + H^+(aq) \qquad K_a = 0.0105 \quad (5)$$

Autoprotolysis of water

$$H_2O \leftrightarrow H^+ + OH^- \qquad K_w = 1 \times 10^{-14} \quad (6)$$

Electroneutrality

$$[Glu^+] + [Na^+] + [H^+] = [Glu^-] + [HSO_4^-] + 2 \cdot [SO_4^{2-}] + [OH^-] \quad (7)$$

Mass balance

$$[Glutot] = [Glu^+] + [Glu] + [Glu^-] \quad (8)$$

The equilibrium was solved from the equations (Eqs. 1–8) in a neutral and acidic pH range where Glu^{2-} ($C_5H_7N0_4^{2-}$) does not exist, as shown in Figure 1. The equilibrium concentration of dissolved Glu^-($C_5H_8N0_4^-$), Glu($C_5H_9N0_4$), and Glu^+($C_5H_{10}N0_4^+$) are included in the overall solubility of glutamic acid and glutamate ions. The calculated equilibrium concentrations were compared to gravimetrically measured data and to the measured values of semi-batch experiments, shown in Figure 2.

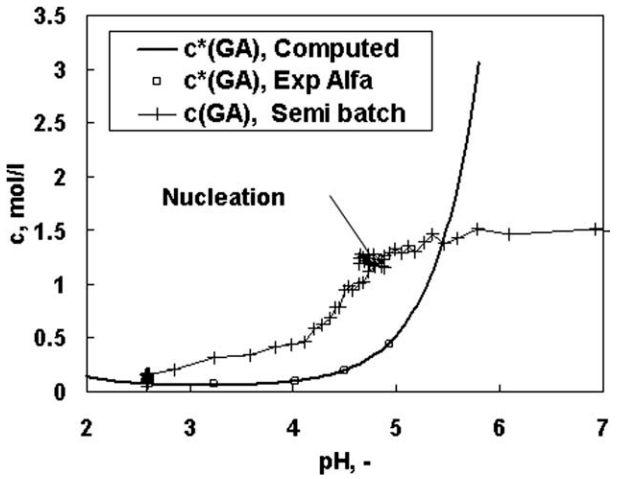

Figure 2. Overall solubility of α-form glutamic acid, c_{GA}*(pH).

Gravimetrically measured values are compared to values solved from thermodynamic equilibrium. An example of measured concentration in a semi-batch experiment is presented.

The sum of the dissociation reaction of Glu[2] and the solid–liquid equilibrium[3] is given in equation.[9] The equilibrium constant or solubility product, $K_{sp,}$ for reaction equation[9] is given in equation.[10] The value for the solubility product was solved from the equilibrium constant of the reaction[2] when a[Glu (aq)] = c*[Glu (aq, α)].

$$\text{Glu (s)} \leftrightarrow \text{Glu}^-\text{(aq)} + \text{H}^+\text{ (aq)} \tag{9}$$

$$K_a = \frac{a(\text{Glu}^-)a(\text{H}^+)}{a(\text{Glu(s)})} = a(\text{Glu}^-)a(\text{H}^+) = K_{SP} = 3.38 \times 10^{-6} \tag{10}$$

One expression for the driving force is the relation of ion product and solubility product (Eq. 11). The activity coefficient $\gamma_\pm$ for the glutamate ion and hydrogen ion can be solved from a modified Bates Guggenheim[1] equation. In this study, the relative supersaturation was solved offline to study its sensitivity as a feedback signal.

$$S = \frac{a(\text{Glu}^-)a(\text{H}^+)}{K_{SP}} = \gamma_{\pm 1}^2 \frac{c(\text{Glu}^-)c(\text{H}^+)}{\left(\frac{\text{mol}}{\text{l}}\right)^2 K_{SP}} \tag{11}$$

The applicability of the relative supersaturation concept as a feedback variable in the closed-loop control was studied and the results are shown in Figure 18.

Solid properties

L-Glutamic acid is known to have two polymorphs (the α-form and β-form) and both forms have two basic shapes. The metastable α-form has prismatic and granular habits and the habits of the stable β-from are needles and flakes.[20] The molecular conformations in the crystal lattice of the α- and the β-form are significantly different through a torsion angle in the main carbon chain,[21,22] and therefore, the polymorphs of L-Glu can be discriminated by Raman spectroscopy.[23] Grant[24(p. 7)] has listed 27 different physical properties generally affected by polymorphs. They are classified to six property categories: packing properties, thermodynamic properties, spectroscopic properties, kinetic properties, surface properties, and mechanical properties.

Kitamura and Ishizu[25] presents the morphological crystal surface structure of the α-form as having a hexagonal surface in directions (001) and (00-1), a rectangular parallelogram in directions (011), (0-11), (0-1-1), and (01-1) and eight trapezoidal surfaces crossing all axes. The shape of the α-L-glutamic acid crystal in Figure 3 is computed with WinXMorph with a distance 1 for each surface, with symmetry assumptions, and with the crystal lattice described in Table 1.

Analysis Methods for Solution and Product Qualities

Spectral analysis of the solution concentration was done using a Bomen MB155 FTIR-spectrometer with a modified Axiom DPR-210 ATR-probe (vertical length 600 mm). The IRE material was AMTIR and it was of conical shape. Spectral variations with a concentration range of dissolved glutamate ion 0.056–1.5 M and with a pH range from 7 to 3 are

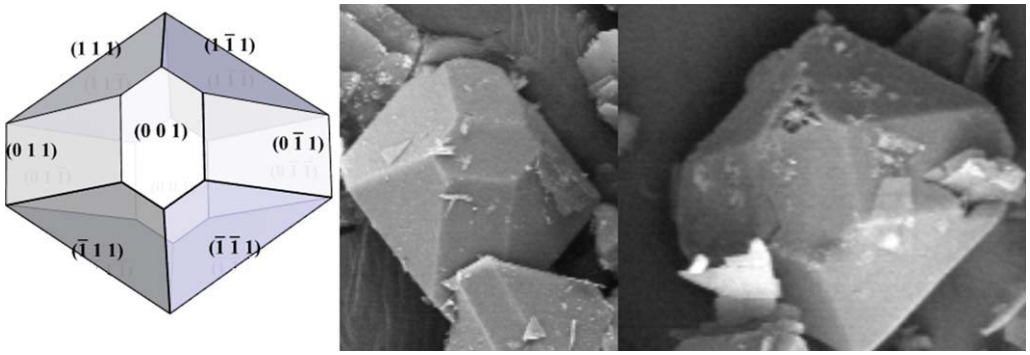

Figure 3. Morphological surface structure of an α-L-glutamic acid crystal and SEM image of an experimental crystal.

[Color figure can be viewed in the online issue, which is available at www.interscience.wiley.com.]

Table 1. Crystal Lattice of Glutamic Acid

	α-form[21] (Å)	β-form[10] (Å)
a	7.068	5.159
b	10.277	17.30
c	8.775	6.948

Crystal lattice of glutamic acid is orthorhombic. Molar mass is 147.13 g/mol. Crystal density is 1.533 g/cm^3.[21]

shown in Figure 4. Modeling of the multivariate model was done with solved thermodynamic equilibrium of equations (Eqs. 1–8) and experimentally measured spectra of solutions in equilibrium with different sulfuric acid additions. Predictive accuracies for the models for glutamic ion and the sum presented with Q^2 values were 99.7% and 99.8%, respectively. The modeling procedure is presented in more detail in Ref. 1. The principles used in the spectral modeling of the ATR-FTIR data are presented by Alatalo et al.[1] The second measured solution property was pH. However, in contrast to experiments in Ref. 1, the crystallization was now done in a 50 L crystallizer. Thus, it was necessary to transfer the calibration for each experiment. For this purpose, 50 samples of stable conditions were utilized.

The qualities of the studied end product were analyzed with three different methods: Raman spectroscopy (Horiba Jobin Yvon LabRam 300), laser diffraction analysis (Beckman Coulter LS13320 with a Tornado dry powder system), and scanning electron microscopy (SEM).

Characteristic peaks of Raman spectra for the α-form of L-glutamic acid are 623, 665, 1003, and 1179 cm^{-1}, and for the β-form 575, 705, 800, 1145, and 1214 cm^{-1}.[23,26] The fraction of the α-form changes the height and the area of the characteristic peaks. The location of the wave number used is shown, together with the Raman spectrum, in Figure 5.

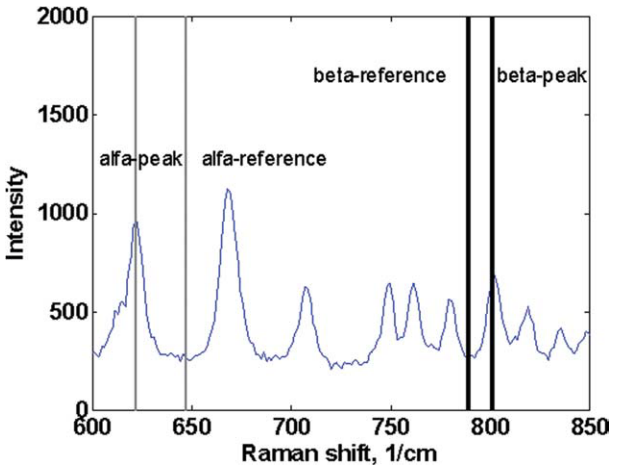

Figure 5. Raman spectrum and locations of used peaks of α-form and β-form of glutamic acid crystals.

[Color figure can be viewed in the online issue, which is available at www.interscience.wiley.com.]

Ono et al.[23] and Qu et al.[9] have used peak height ratio to compute the mass fraction of the α-form. Fitting of the 2nd degree polynomial (Eq. 13) of the peak height ratio of Eq. 12 was done with mixtures of pure α-form and β-form crystals, see Figure 6. The mass fractions of the α-form in the mixtures used in the calibrations were 0.00, 0.25, 0.50, 0.75, and 1.0.

$$x = \frac{\text{Peak}(622) - \text{Peak}(647)}{[\text{Peak}(622) = \text{Peak}(647)] + [\text{Peak}(801) - \text{Peak}(789)]} \tag{12}$$

$$\alpha(\text{mass fraction}) = ax^2 + bx + c \quad a = -40, b = 140, c = 0.43 \tag{13}$$

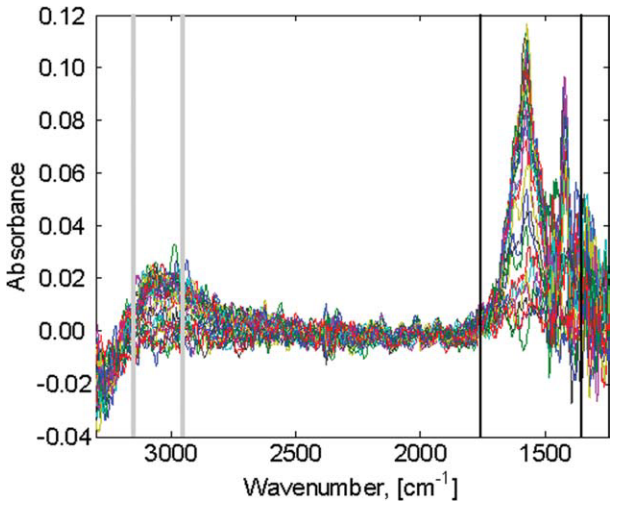

Figure 4. Original ATR-FTIR spectra and two wave number range used in the model.

[Color figure can be viewed in the online issue, which is available at www.interscience.wiley.com.]

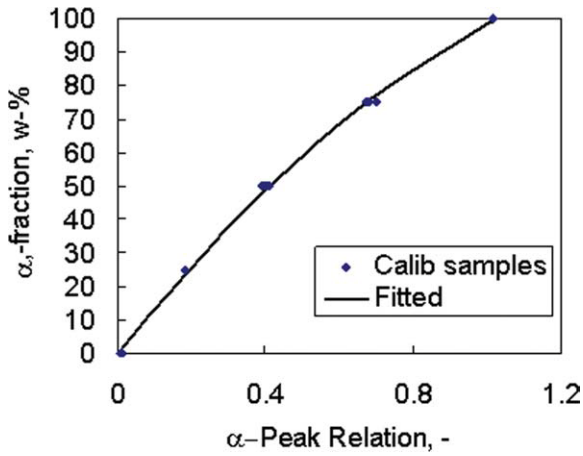

Figure 6. Polynomial fitting of α-form mass fraction and Raman peak ratio, R^2 = 0.9996.

[Color figure can be viewed in the online issue, which is available at www.interscience.wiley.com.]

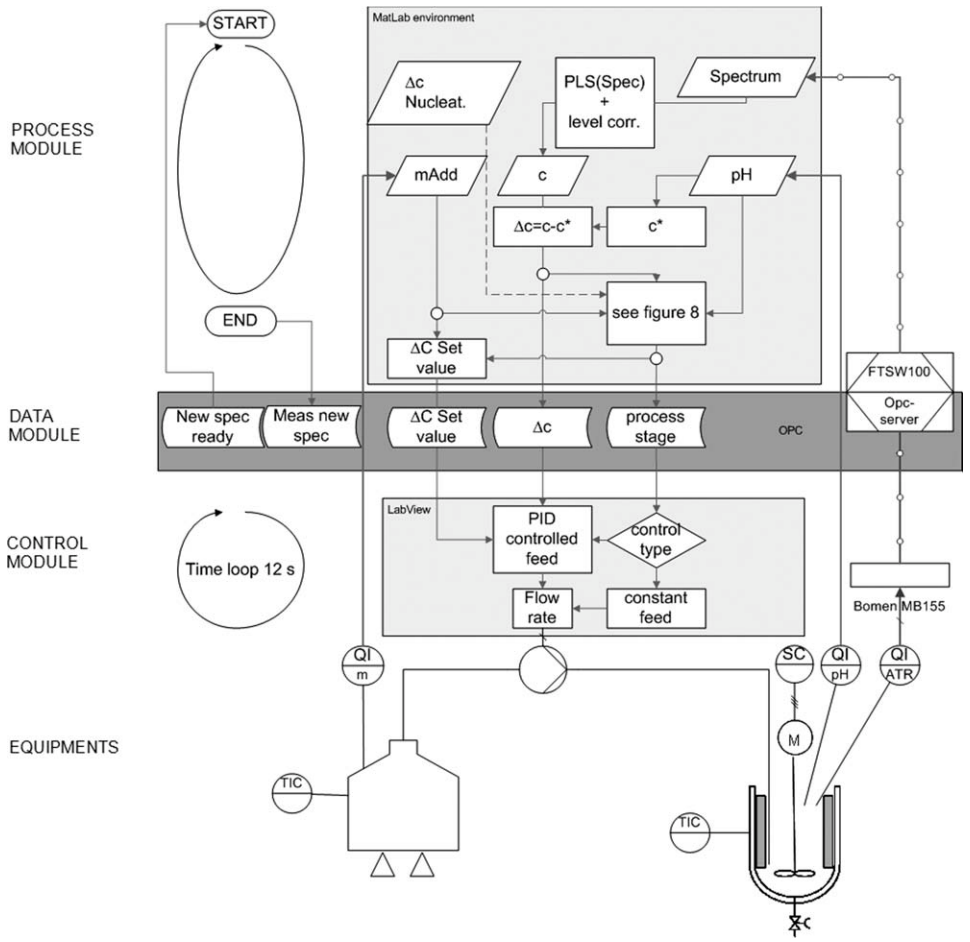

Figure 7. Experimental setup and principles of the information flow of the control system of the 50 L crystallizer setup.

FTSW100 is used to collect spectrum.

Pure α-form crystals were produced by adding 6.85 mL 1.65 M H_2SO_4 to a 100 mL 1.5 M MSG solution. The crystals were filtered after 5 min mixing with a magnetic stirrer and washed three times with ethanol (99.5 wt %) to prevent polymorph transformation.

Description of Process and Crystallizer

The crystallization process used in this study included all necessary equipment to execute proper feed to the crystallizer, crystallization, and sending forward product crystals as a suspension. The decision to use a semi-batch process means the study has concentrated on unsteady state unit operations whose characteristic behavior is that solution and suspension properties like volume, concentration, viscosity, etc., are in dynamic change. Population density $n(L)$ changes because of nucleation, growth, breakage, and agglomeration. Dynamic changes in suspension and solution properties are produced by kinetic phenomena present inside the crystallizer. In the order in which they occur in the crystallization process, these phenomena are: kinetics of mixing, kinetics of reactions, kinetics of crystallization, and kinetics of polymorph transformation. The kinetics occurs simultaneously with unsteady state heat transfer operation.

Construction of a crystallizer has to meet three aims: mixing of the reagents after feed, mixing of the suspension to homogenize suspension density, and temperature control of the suspension. The mixing arrangements are a combination of impeller type, stirring rate, crystallizer geometry, and feed conditions. Feed of the reagent consists of location (different locations at different process stages), direction of feed flow, nozzle geometry, and flow rate of the reagent. Flow directions together with micromixing and macromixing rates are a consequence of geometrical details (nozzle, shape of the vessel, mixer type, and baffles), suspension properties (viscosity of the mother liquor, density and size of the solids, and suspension density), and kinetic energy (mixing power and kinetic energy of feed flow).

Keeping the temperature at a constant level is difficult because of dilution enthalpy, reaction enthalpy, and phase change. In this study, temperature control was based on heat transfer through the glassy wall of the jacket. The cooling rate needed can be decreased by precooling of the feed with a separate temperature control unit, see Figure 7.

Control System

Process control of crystallization requires sensors, analyzers, data processing programs, controllers, and actuators. Despite automatized operations, some user controlled actions still remain. The driving force of reactive crystallization, supersaturation, is produced by the addition of a reagent (H_2SO_4). The level of supersaturation can be controlled with the feed rate. Mixing phenomena and the mechanisms of heterogeneous nucleation mean the feed nozzle location must be controlled to prevent uncontrolled nucleation at the liquid surface or inside the nozzle. In the present study, feed rate control was automatic, as explained below, and feed location control was manual.

Many measurements have been used in situ to study the behavior of crystallizers, for example: pH, temperature, conductivity, turbidity, ion selectivity, particle size, ATR-FTIR spectra, and Raman spectra. H^+-ion concentration and conductivity is connected to too many reactions or compounds to permit its use to describe concentration alone. Temperature measurement can be used to follow a time dependent set point trajectory or to keep constant temperature with a thermostating unit. Ion selective electrodes exist for some inorganic compounds. Turbidity can be used to detect nucleation or solid concentration with low suspension densities.[27] Li et al.[28] have analyzed the size and fraction of the α-form of glutamic acid crystals based on shape factors computed with an in situ image analyzer. This method could possibly be used to analyze end product quality when the product consists mostly of the needles-type β-form and prismatic α-form of glutamic acid. The ability of Raman spectroscopy to produce concentration information for control purposes is probably under investigation in many research laboratories at this moment. For glutamic acid, a FTIR spectrometer with an ATR—probe seems a promising tool to measure concentration online and in situ for control purposes.[1–4,8,29–31] This study is based on using ATR-FTIR to measure concentration in situ. Khan et al.[4] and Grön et al.[31] have used similar ATR-FTIR measurements in a feedback connection of a control structure when they studied closed loop cooling crystallization of L-glutamic acid and monosodium glutamate (MSG).

Process stages

Recognition and classification of different process stages, which should be based on different control principles, play a key-role in the control structure, see Figure 8. Some preliminary preparations and post processing, like measurement of the background spectrum from pure solvent, in this case water, were manually controlled procedures.

In a reactive semi-batch crystallization process, the time from beginning of feed to beginning of nucleation has three different periods; first, the time during which the solution is unsaturated, second, the time during which the supersaturated solution undergoes increasing supersaturation (to set value) and third, the waiting time before nucleation without reagent addition at the desired supersaturation level.

The nucleation moment is in practice followed by a waiting period before the control system recognizes the nucleation using pH criteria. This study only considers spontaneous primary nucleation. The primary nucleation is followed by a PID controlled feed period of growth and secondary nucleation. The optimal endpoint of the reagent feed is based on the mass of the added reagent or measured solution properties like pH.

When considering feed flow rates and feed locations at different process stages, attention must be paid to the following details. First, flow is not allowed to stop when the nozzle is below the surface. This is important to prevent back diffusion to the feed pipe and plugging of the nozzle because of the nucleation and growth of crystals. The small characteristic diameter of the flow channel produces a high flow velocity at the nozzle. Together with conical shape of the nozzle, the high flow velocity prevents unwanted flow behavior and nucleation. A second important detail is that flow has to be stopped when the nozzle is above the liquid surface to prevent heterogeneous nucleation at the surface because of liquid- and gas-steel interface connections and poor mixing at the liquid surface.

Control structure

The studied control principle was closed loop control with a PID-controller. A feedback connection was built from the measured solution properties to the analogical control signal of the peristaltic pump.

The programmed control structure, see Figure 7, was built up using the following software tools: FTSW100, MatLab, LabView and an OPC-server. The structure includes four independent task groups, namely, spectrum collection, the control module, the process module, and the data module. FTSW100 software and the OPC-server were installed in a computer with a spectrometer connection. Matlab and Labview were installed in a computer with a connection to a pH analyzer, balance, and peristaltic pump. The computers were connected with a safe LAN connection for OPC-connections and spectral data transfer.

Spectrum collection was done with FTSW100 software. Measurement of a new spectrum was synchronized with the process loop based on digital I/O variables of the data module. The OPC-server was used to deliver and update the values of dataset variables, gray color in Figure 7. The control module, programmed in LabView, directed the analytical control signal of the feed pump based on the PID. The time step of discrete control was chosen so that input values of the PID controller were updated for every time step.

The task of the process module, Figure 7, which operated with MatLab, was to collect data values from the analyzers and compute valid process stage values, set values and feedback values and to write those values to the data module. The process stage decision (see Figure 8 and list below Table 2) based on pH, reagent addition, set value, and feedback signals was used to compute the set value in the process module. Multivariate model analysis of the ATR-FTIR spectra was used to compute the concentrations needed in computation of the feedback value.

Control in the set point trajectory experiments was based on glutamate concentration and pH measurement. The volume of added acid was integrated from the feed rate value of the peristaltic pump. The accuracy and stability of the concentration data used to compute supersaturation is

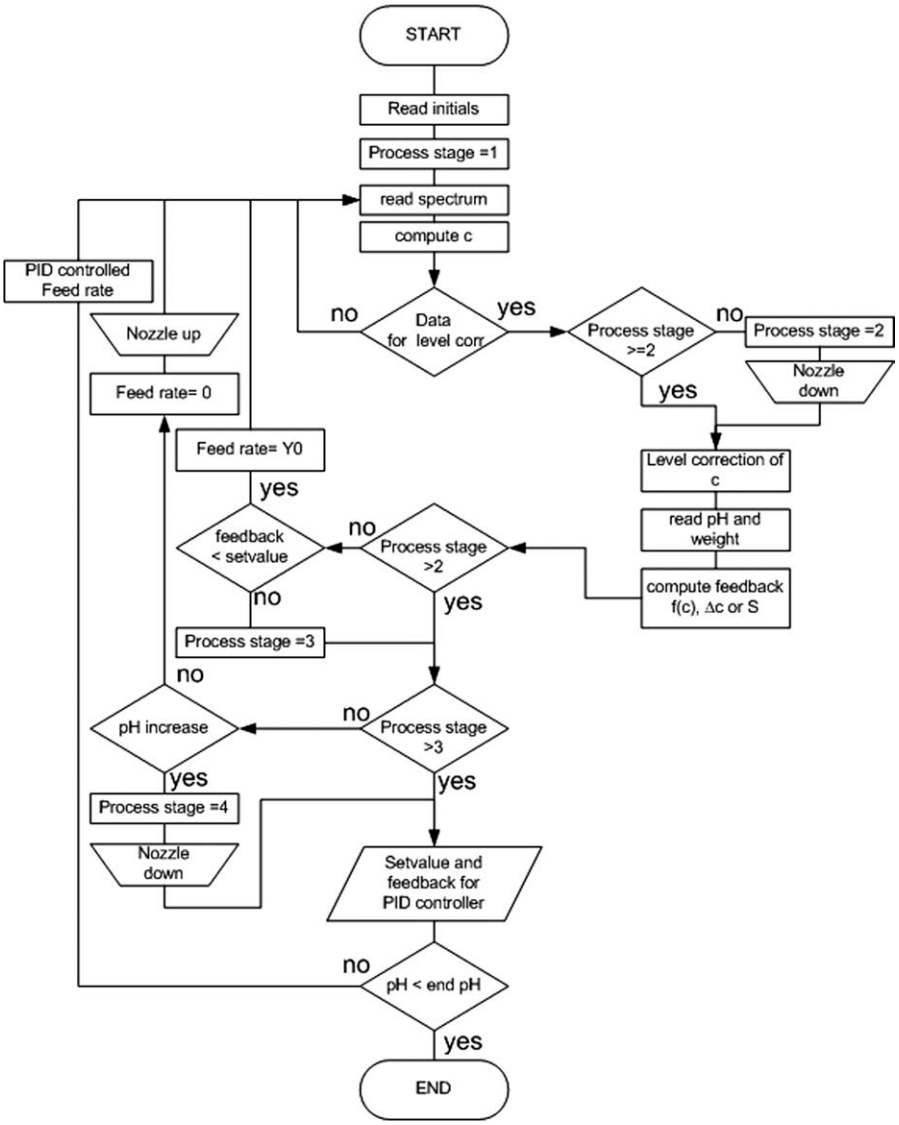

Figure 8. Flow chart of process stage decisions of control structure.

See also Figure 7 and list at next page.

important for the control system. Concentrations measured with FTIR-ATR had a specific level of instability. Random variation of the measured supersaturation was too high at a level in the case where the driving force was based on the solid–liquid equilibrium reaction (Eq. 3). For this reason, control of the experiments in a 50 L crystallizer was based on measured overall concentration of the dissolved glutamic acid group, pH, and mass of added acid. The feedback signal of the closed loop control system was the difference between the overall concentration measured with ATR-FTIR and the overall concentration at equilibrium at measured pH computed from polynomial fitting shown in Figure 2.

Table 2. Details of Nozzle Diameter and Flow in the Experimental Work

Set point trajectory experiments in 1 L crystallizer	Δc-controlled experiments in 50 L crystallizer
Nozzle diameter 0.4 mm Max flow rate 0.8 g/s, 5.8 m/s	Nozzle diameter 2.0 mm Flow before nucleation a. 2.8 g/s, 0.8 m/s b. 5.0 g/s, 1.45 m/s c. 8.6 g/s, 2.5 m/s Flow after nucleation Max 18 g/s, 5.22 m/s

$$\Delta c = c(\text{Gul (aq)}) + c(\text{Glu}^- \text{ (aq)}) - c^*(\text{Glu (aq)}) - c^*(\text{Glu}^- \text{ (aq)}) \quad (14)$$

Experimental Procedures

Experiments were carried out on two scales, a 1 L and 50 L crystallizer, with the same crystallizer geometry and the same type of impeller. Chemical and geometrical details of the experimental study are given in Table 2 and in Table 3.

Table 3. Chemical and Geometrical Details of the Experimental Work

	Calibration	Set Point Trajectory of $c(Glu^-)$ Controlled Experiments	Δc-Controlled Experiments
Volume and diameter of crystallizer	1 L 100 mm	1 L 100 mm	50 L 300 mm
Volume, mass, and concentration of initial batch	0.650 L 713 g 1.5 mol (MSG)/L	0.650 L 713 g 1.5 mol (MSG)/L	13.05 L 14.665 kg 1.5 mol (MSG)/L
Total volume of added 1.5 M acid	Different additions	0.350 L 384 g	5.9–6.3 L 6.5–6.9 kg
Quality of MSG	L-Glutamic acid, Monosodium salt, Monohydrate, 98% (Aldrich)	L-Glutamic acid, Monosodium salt, Monohydrate, 98% (Aldrich)	Monosodium, Glutamate, 99% (Sonochen Ningbo LTD)
Quality of H_2SO_4	95–97% pro analysi (Merck)	95–97% pro analysi (Merck)	95–97% pro analysi (Merck)
Water	Millipore (0.054 μS/cm)	Millipore (0.054 μS/cm)	Deionized (1 μS/cm)
Mixer	Pitched up pumping six-blade turbine ($d = 50$ mm)	Pitched up pumping six-blade turbine ($d = 50$ mm)	Pitched up pumping six-blade turbine ($d = 150$ mm)
Mixing rate	500 rpm $Re = 5500$–10,600 Tip speed = 1.31 m/s	500 rpm $Re = 5500$–10,600 Tip speed = 1.31 m/s	167 rpm $Re = 15{,}000$–39,000 Tip speed = 1.31 m/s

In the set point trajectory experiments, the feed flow rate was controlled with PID from the beginning of the experiment. The flow rate of feed before the set value reached in Δc-controlled experiments was used as a variable in the experiments. Temperature in all experiments was 25°C.

Initialization of a spectrometer requires measurement of the background with a thermostated solvent and measurement with a thermostated initial batch of the required level correction for the calibration model. Background and level correction were measured for each experiment in the crystallizer. As a fundamental starting point, there are two aspects to the importance of crystallizer purity. To be sure about the mechanism of nucleation, the crystallizer has to be free from solid contaminations. Second, measurement of the ATR-FTIR background spectrum of the pure water requires that dissolved impurities do not exist. Preliminary preparations included preparing thermostated solutions for the initial batch ($T = 25$°C) and feed reagent ($T \approx 8$°C). The feed acid was cooled to about 17°C below the temperature of the crystallized solution to minimize temperature increase caused by dilution enthalpy and reaction enthalpies.

Macro mixing in the experiments was produced with an up-pumping pitched six-blade turbine (mixer and tank diameter relation $d/D = 0.5$) and four baffles. The constant tip speed of the impeller was 1.31 m/s. The feed nozzle was located near the impeller, at the point of highest micromixing in the crystallizer. Feed flow was stopped and the nozzle lifted when the set value was reached. When the control system had recognized that nucleation had started, the nozzle was relocated near the impeller.

1. Level correction of the multivariate model.
2. H_2SO_4 (1.5 M) addition with a constant flow rate (Table 2) until the set value for ΔC is reached (1–3 min). Nozzle near impeller.
3. Waiting for spontaneous nucleation (15 s–5 min). Nozzle above liquid level.
4. Period of controlled feed of reagents (10–50 min). Nozzle near impeller.
5. End of feed. Nozzle above liquid level.
6. Degradation of supersaturation and possible polymorph transformation immediately following reagent addition is stopped.
7. Samples are taken 1 min after nucleation and at the end of reagent feed. For some of the experiments, additional samples are taken with a 10 min time step.

Set value principles

The start of nucleation in a solution is followed by a decrease in the concentration of the crystallized compound in the mother liquor. Simultaneously, the maximum supersaturation level decreases. In the case where the set value was constant, the supersaturation level remained below the set value during the end period of the crystallization. This causes reagent feed with maximum flow rate. The crystallization kinetics of glutamic acid is relatively slow which produces a long time period with minimum feed rate if the set value is decreased to a low value soon after nucleation, gray line in Figure 9. In the present study, control with a linearly decreasing set value (as a function of the added reagent mass) was compared to a constant set value and a constant set value with step change. In practice, the new set value of the linearly decreasing case was computed only when measured Δc was below the set value.

Results

Dynamic changes of solution and suspension properties

The dynamic nature of a semi-batch crystallizer can be understood with Figures 10 and 11, where experimental

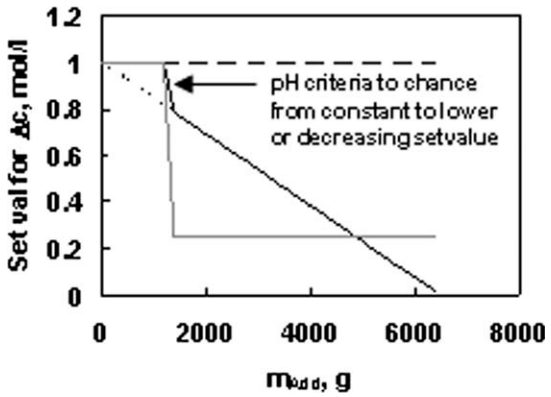

Figure 9. Control strategies for period of growth and secondary nucleation.

m_{Add} is mass of added 1.5 M sulfuric acid.

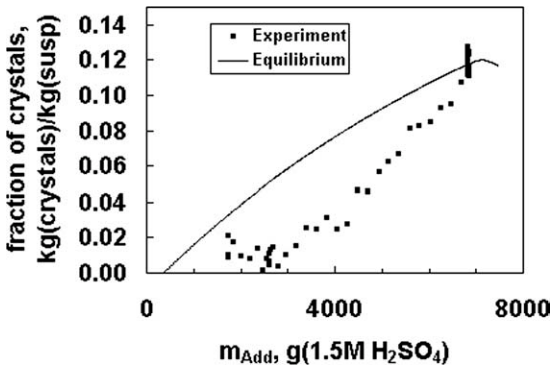

Figure 10. Solid mass fraction in suspension.

values are compared to equilibrium values of the semi-batch experiment, see Δc controlled experiments of Table 2 for details. The difference in the mass fraction of the crystals in the suspension between the equilibrium and semi-batch crystallization experiment can be seen in Figure 10. The concentration of the crystallized compound decreases simultaneously with increasing suspension density.

The mass fraction of dissolved (w_{dis}) glutamic acid including Glu(aq) and Glu^-(aq), follows the equilibrium computed without the solid–liquid equilibrium before nucleation, the thicker black line in Figure 11. Thinner line is computed with the solid–liquid equilibrium (Eq. 3). After nucleation, the overall concentration goes slowly toward equilibrium with the solid–liquid equilibrium. The concentration of those dissolved species which do not crystallize increases because of sulfates in the feed (Figure 11).

The present study does not focus on modeling the kinetics, but the following aspects of kinetics were considered. Temperature was kept constant to minimize variation because of temperature dependent kinetics of nucleation, growth, and polymorph transformation. Acid base reactions are fast compared to crystallization kinetics, which means that phase change, nucleation, and growth control the reaction and there is no reason to focus on reaction kinetics of acid base reactions. After the induction time, when nucleation starts, degradation of the driving force begins. It is possible to find two time moments which connect nucleation and growth to feed rate, and local minimum and maximum of pH just after nucleation. This is valid especially with a constant feed rate (see Figures 12, 13, and 17). At those time moments, the feed produces the same amount of H^+ −ions as the crystallization consumes.

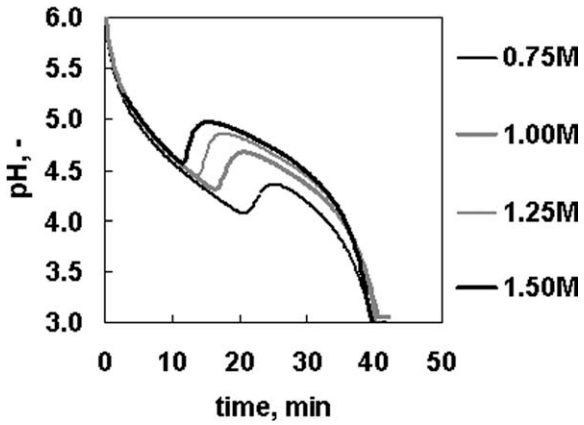

Figure 12. pH behavior in semi-batch crystallization with constant feed flow (8 mL/min).

Volume of crystallizer was 1 dm^3 and volume of initial batch was 0.650 $dm.^3$ Mixing rate 500 rpm with propeller.

The dynamic behavior of pH in Figures 12 and 13 are from four different types of experiments. Experiments with constant feed flow are shown in Figure 12, and experiments based on set point trajectory of c(Glu^-) and Δc-controlled experiments are given in Figure 13. In the set point trajectory experiments, the flow rate was controlled with PID from the beginning of the experiment. In the Δc-controlled experiments, the flow rate was 8.3 g/s before the set value was reached.

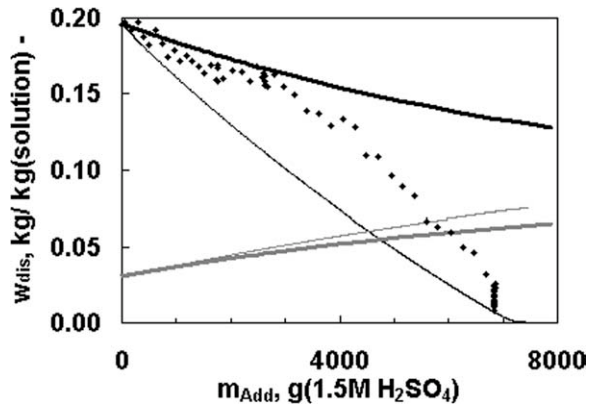

Figure 11. Fraction of dissolved compounds in mother liquor.

The black line is for glu(aq) + glu^-(aq) and the gray line is for the sum of dissolved Na^+- and SO_4^{2-}-ions in the equilibrium. Thicker lines do not take account the solid–liquid equilibrium. Dots are experimentally measured values for glu(aq) + glu^-(aq).

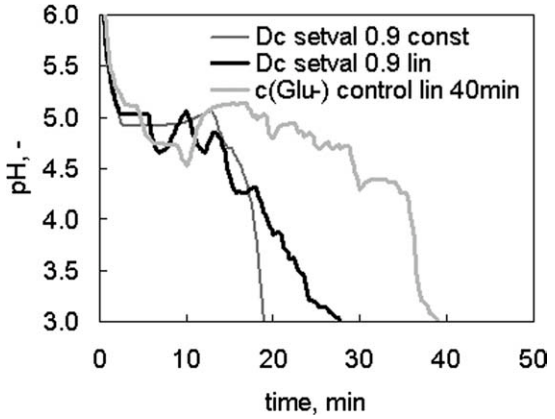

Figure 13. pH behavior in semi-batch crystallization with set point trajectory of c(Glu^-) controlled feed and with supersaturation Δc(c(Glu)+c(Glu^-)) controlled feed.

Solutions were 1.5 M. See Table 2 and Figure 15 for details.

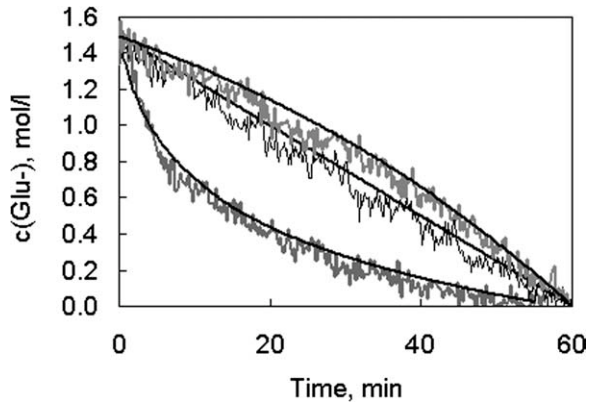

Figure 14. Controllability of concentration with time dependent set point trajectory of c(Glu$^-$).

See Table 3.

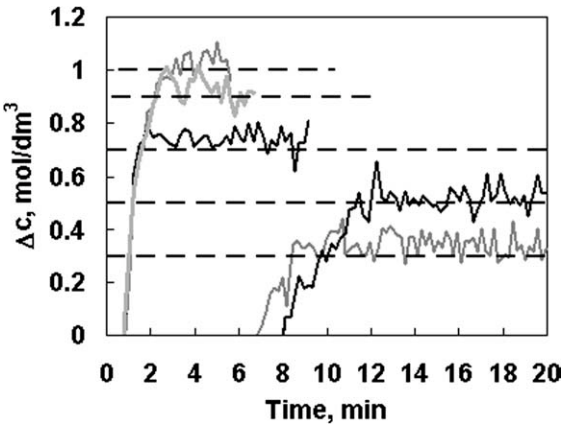

Figure 16. Controllability of Δc levels for primary nucleation.

Set value levels 0.7, 0.9, and 1.0 were used with the flow rate 8.6 g/s and set value levels 0.3 and 0.5 with the flow rate 0.8 g/s before the supersaturation level reached the set value. See Table 2.

Set point trajectories

Indirect control of the driving force of crystallization is based on a measurable quantity like temperature or concentration. Concentration itself is not the driving force, but time dependent change of concentration is connected to the formation rate of the driving force. When the concentration set point trajectory is connected as a function of another measured quantity like temperature[4] or pH to the metastable area concentration, the control systems produce controlled supersaturation.

In the present study, the time dependent set point trajectory was studied as a preliminary step toward control of supersaturation. Controllability of c(Glu$^-$) was rather good, see Figure 14. When the concentrations are shown as a function of pH, Figure 15, the effect of the set point trajectory type on nucleation pH can be analyzed.

Control of supersaturation

Control based on the difference in the overall concentration of glutamic acid and the equilibrium value of overall concentration, Eq. 15, was successful, see Figure 16. Controllability of the supersaturation level can be considered separately for different process stages; the period of primary nucleation, and the period of growth and secondary nucleation (see Figures 16 and 17).

Random variation in the measured supersaturation level imposes limitations on the accuracy of the measurement method. The period of secondary nucleation and growth shows two interesting behaviors of pH as a consequence of the slow crystallization compared to the reaction. The increase of pH in Figure 17 indicates a decrease of supersaturation (Eqs. 2 and 3). The decrease of pH is connected to the progress of the semi-batch process with equations of equilibrium (Eqs. 1–8) and to the formation of supersaturation (see Figure 2).

The concentration and supersaturation behavior during the experiments can be compared in Figures 18–23, where measured concentration, supersaturation, and pH data are presented together with the set value, equilibrium concentration, and relative supersaturation. The relative supersaturation was computed from Eq. 11 with a value 0.79 for the activity

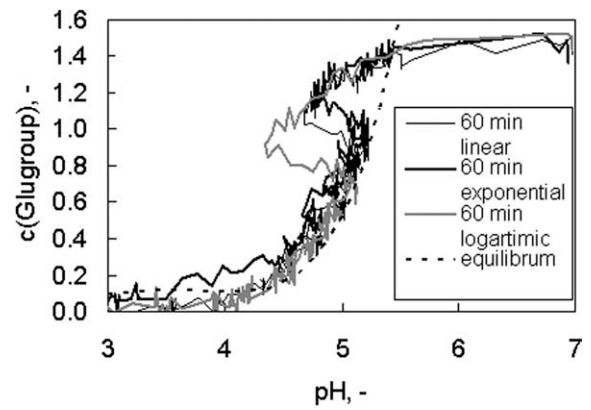

Figure 15. Concentration behavior in set point trajectory controlled experiments.

See Table 2.

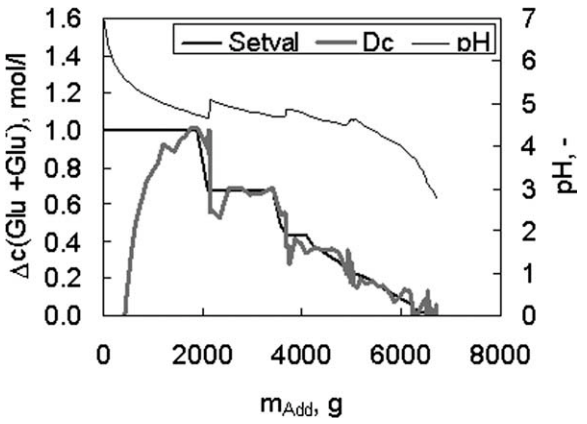

Figure 17. Controllability of super-saturation at the period of secondary nucleation and growth.

See Table 2.

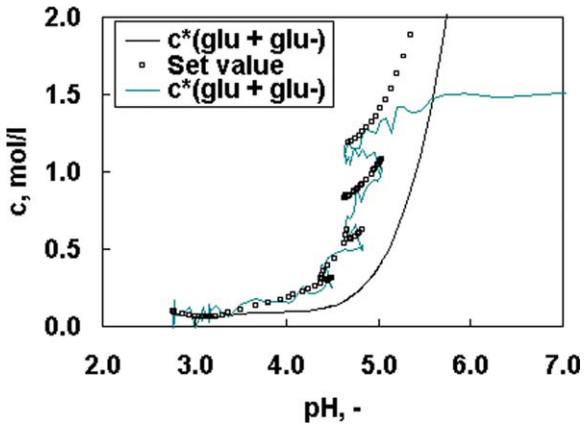

Figure 18. Set value, concentration and equilibrium concentration as a function of pH in the experiment where the set value for primary nucleation was 1 mol/L and linearly decreasing for the growth period.

The feed rate was 8.6 g/s before the set value was reached. For further details of the experiment, see Δc-controlled experiments in Table 2. [Color figure can be viewed in the online issue, which is available at www.interscience.wiley.com.]

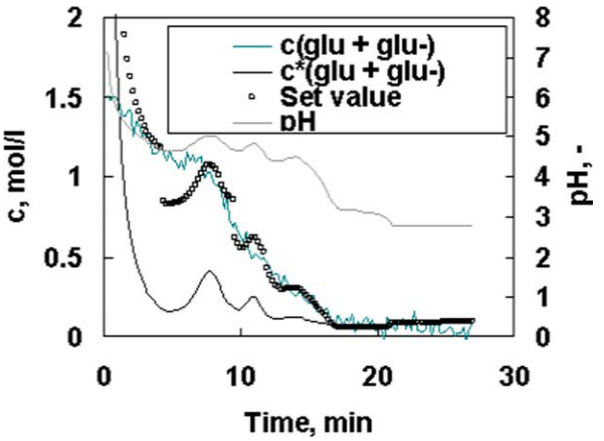

Figure 20. Set value, concentration, pH and supersaturation as a function time in the experiment where the set value for primary nucleation was 1 mol/L and linearly decreasing for the growth period.

The feed rate was 8.6 g/s before the set value was reached. For further details of the experiment, see Δc-controlled experiments in Table 2. [Color figure can be viewed in the online issue, which is available at www.interscience.wiley.com.]

coefficient for the glutamate and hydrogen ions. All values in Figures 18–23 were computed for one experiment. Time and mass of added sulfuric acid are independent variables but pH is a function of the added mass of sulfuric acid and time used for the addition.

Set value behavior in Figures 18–21 shows that a constant set value for Δc means an increasing set value for concentration when pH is increasing because of the low feed rate of sulfuric acid. Relative supersaturation (Eq. 11) has a linear response to the added mass of reagent before nucleation. After nucleation, the up to 5000 g addition response seems to be logical. At the end of addition, the response differs strongly from the Δc response to the control of reagent addition.

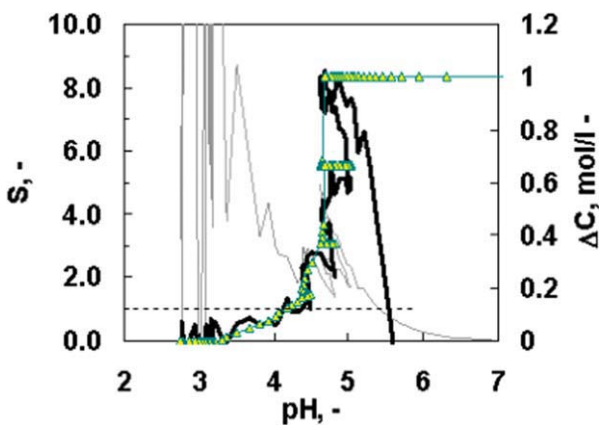

Figure 19. Set value and supersaturation together with relative supersaturation as a function of pH in the experiment where the set value for primary nucleation was 1 mol/L and linearly decreasing for the growth period.

The feed rate was 8.6 g/s before the set value was reached. For further details of the experiment, see Δc-controlled experiments in Table 2. [Color figure can be viewed in the online issue, which is available at www.interscience.wiley.com.]

Effect of Process Control on Crystal Quality

The studied properties of the product crystals were polymorph and size. The habit of the α-form and β-form product

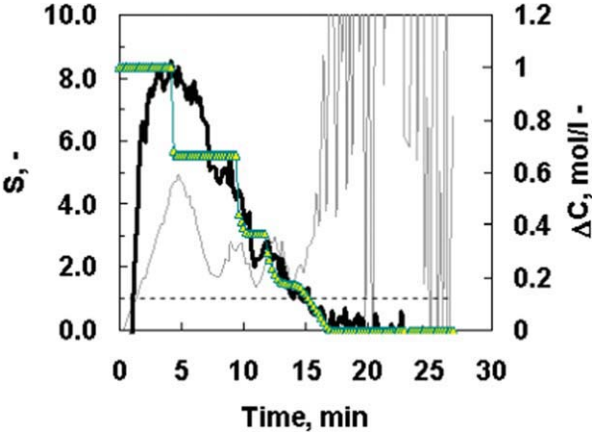

Figure 21. Set value and supersaturation together with relative supersaturation as a function of time in the experiment where the set value for primary nucleation was 1 mol/L and linearly decreasing for the growth period.

The feed rate was 8.6 g/s before the set value was reached. For further details of the experiment, see Δc-controlled experiments in Table 2. [Color figure can be viewed in the online issue, which is available at www.interscience.wiley.com.]

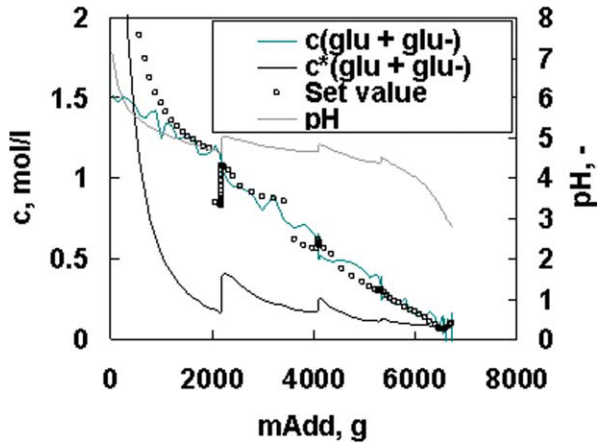

Figure 22. Set value, concentration, pH and equilibrium concentration as a function of mass of added sulphuric acid in the experiment where the set value for primary nucleation was 1 mol/L and linearly decreasing for the growth period.

The feed rate was 8.6 g/s before the set value was reached. For further details of the experiment, see Δc-controlled experiments in Table 2. [Color figure can be viewed in the online issue, which is available at www.interscience.wiley.com.]

crystals are shown in SEM-images, Figure 24. The quality for the polymorph content was described with the mass fraction of the a-polymorph (Table 4 and Figure 28). Size was analyzed by comparing mean size, Table 4, and crystal size distributions (CSD), Figure 25.

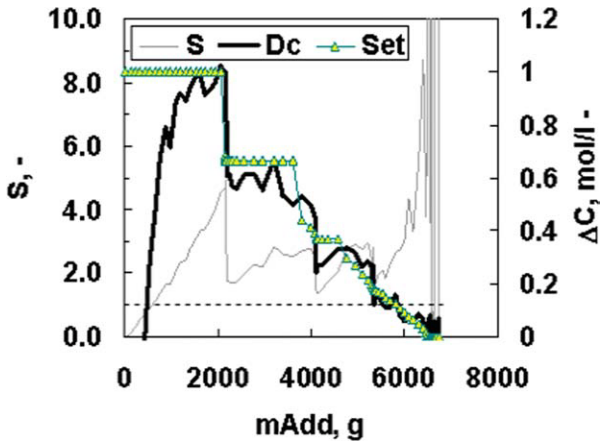

Figure 23. Set value and supersaturation together with relative supersaturation as a function of added sulphuric acid in the experiment where the set value for primary nucleation was 1 mol/L and linearly decreasing for the growth period.

The feed rate was 8.6 g/s before the set value was reached. For further details of the experiment, see Δc-controlled experiments in Table 2. [Color figure can be viewed in the online issue, which is available at www.interscience.wiley.com.]

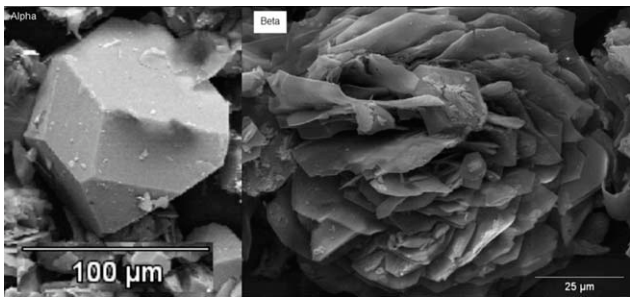

Figure 24. SEM images of the α-form and β-form glutamic acid crystals.

A number of sedimentation experiments were done to compare the settling velocities of the α and β forms and the fraction of clear liquid after settling as a function of the mass fraction of the α-polymorph (see Figure 26). When the crystals are pure β-form there is no settling at all.

The shape of the CSD, Figure 26, changes from unimodal to bimodal when the product crystal polymorph changes from α to β. Mean size of the particles increases when the set value of Δc for the primary nucleation and feed rate before nucleation increases (Table 3). The range of maximum diameter of α-form L-glutamic acid crystals in Figure 27 is 20–100 μm. Reference values for crystal size in the case of cooling crystallization are taken from literature. The range of maximum diameter of the crystals in images of Kee et al.[5] was 260–460 μm. Li et al.[28(p. 843)] published a mean length of crystals of about 110 μm. The maximum diameter of pH-shift precipitated crystals in the SEM—image of Schöll et al.[6] was 60–325 μm.

The measured polymorph contents with different set values are presented in Figure 28. In the figure, experiments with a low set value (below 0.8) used a low feed rate before nucleation. Experiments with a high set value used both low and high feed rates. High supersaturation levels could not be attained with low feed rates because of the short induction time.

The stability of the product crystals in mixed product suspension after crystallization was analyzed. Results show that in many experiments, a sample taken at the end moment of reagent addition and sample taken 20 min after the end of reagent addition has the same fraction of α-form crystals. Two experiments were tracked up to 80 min after the end of

Table 4. Fraction of α-Polymorph and Mean Size of Product Crystals

Set Value of Δc for Primary Nucleation (mol/L)	Feed Rate Before Nucleation (g/s)	Time to Set Value (min)	α-Fraction (w-%)	Mean Size (μm)
0.3	0.8	8.5	0	37.08
0.5	0.8	4.6	0	34.03
0.7	0.8	14.7	0	37.14
0.9	8.3	2.5	17	35.47
1.0	0.8	26.7	1	34.52
1.0	2.8	11.3	16	67.73
1.0	5.2	4.6, 4.4	37	51.42
1.1	8.3	5.0	61	74.88

For experimental details, refer Table 2, column Δc-controlled experiments.

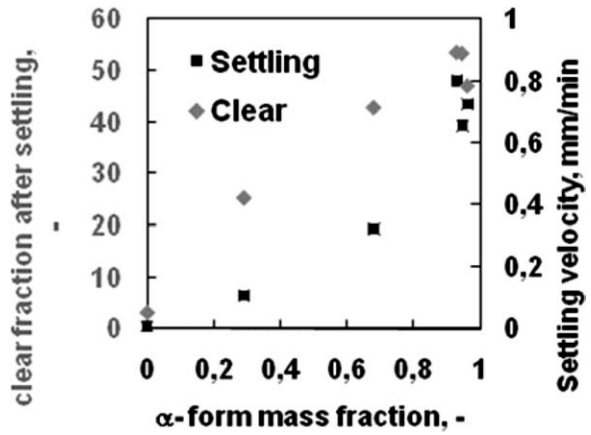

Figure 25. Crystal size distribution of product crystals of Δc-controlled semi-batches.

Crystal size was analyzed by Beckman Coulter LS13320 with a Tornado dry powder system.

the feed stage and no clear decrease in the α-fraction was found.

Conclusions and Discussion

Semi-batch reactive crystallization of L-glutamic acid by adding sulfuric acid produces a flake-shaped crystal habit for the β-polymorph and a prismatic habit for the α-polymorph. The initial aqueous solution contained monosodium glutamate. The shape of the CSD obtained by laser diffraction particle size analysis indicates the polymorph. The differences between these two polymorphs were clear in the crystal shape obtained with SEM and the sedimentation nature. Crystal polymorphs were analyzed with a Raman spectrometer.

The mean size of the product increases when the mass fraction of the α-form increases. A higher supersaturation level has to be used to produce α-form crystals. A high feed flow rate of acid reagent before nucleation was needed to reach such high supersaturation.

The developed closed-loop process control system allowed the glutamate ion concentration to be adjusted according to

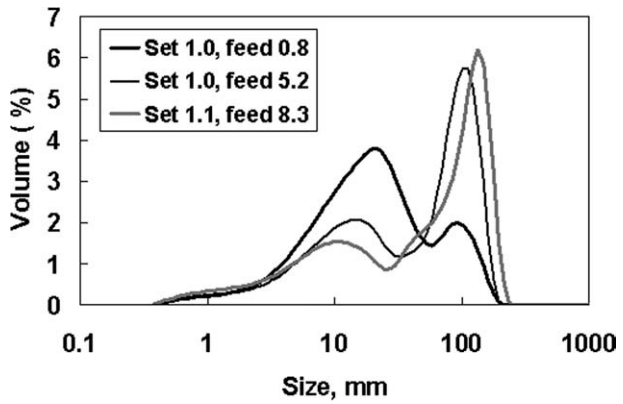

Figure 26. Settling behavior of product suspension in a 100 mL measuring glass.

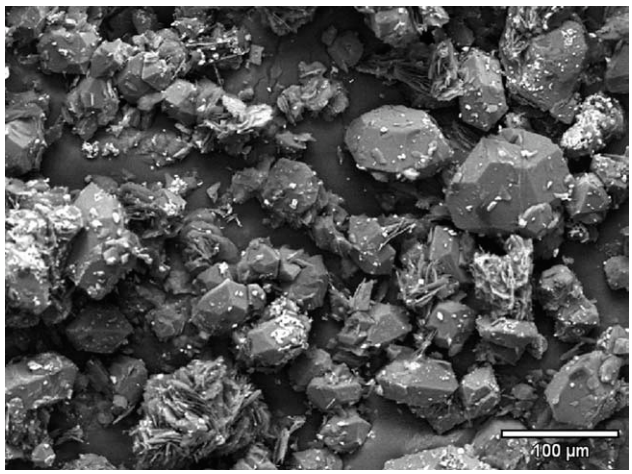

Figure 27. SEM image of product crystals from the experiment with a set value 1.1 for primary nucleation and a linearly decreasing set value at the period of growth and secondary nucleation.

time dependent pre-defined set point trajectories. This was shown experimentally in a 1 L crystallizer. In a 50 L crystallizer, the supersaturation level of the overall concentration of glutamic acid (Glu + Glu^-) at the initiation moment of primary nucleation was successfully controlled. Further, the supersaturation level at the growth stage could be controlled to some extent.

The supersaturation level after primary nucleation affects the α–β phase transformation and crystal growth. In the case where the supersaturation level was decreased to a low level, 0.15 mol/L, after nucleation at a high supersaturation level, 1 mol/L, the mass fraction of the α-form in the product crystals decreased to zero.

The obtained results showed that the feedback process control approach developed for semi-batch precipitation allows control of both the form of the polymorphs and the crystal size distribution. On the basis of the results obtained,

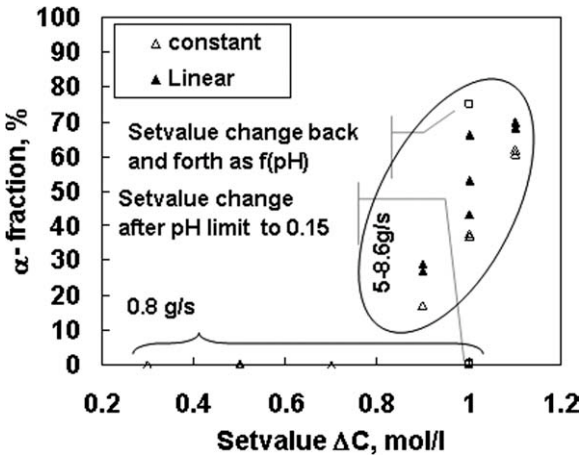

Figure 28. Effect of process control on the mass fraction of α-form glutamic acid in the product.

Flow rates before the set value was reached are shown.

the supersaturation level at the nucleation moment affects almost linearly the polymorphic composition. It was noticed that the relative supersaturation computed from the measured results gives promising results from the viewpoint of feedback control. For the studied compound system, fixing the relative concentration, $[Glu^-][H+]/K_{SP}$, seems to be favorable for process control.

Acknowledgments

The authors thank the Finnish Funding Agency for Technology and Innovation (Tekes) and collaborating companies in the PAT Kiva project, the Academy of Finland (Projects Nos. 211014 and 117155), and Lappeenranta University of Technology Research Foundation for financial support. Docent Jaakko Partanen from Lappeenranta University of Technology is acknowledged for his guidance and discussions concerning the thermodynamics study. Mr. Mikko Huhtanen is acknowledged for his guidance concerning morphology modeling. Dr. Haiyan Qu is acknowledged for her valuable assistance with polymorph analysis using Raman spectroscopy. The authors are grateful to Ms. J. Carrasco Danés, Ms. Y. Dai, and Mr. Morgan Thebault for their assistance in carrying out the kinetic precipitation experiments.

Literature Cited

1. Alatalo H, Kohonen J, Qu H, Hatakka H, Reinikainen S, Louhi-Kultanen M, Kallas J. In-line monitoring of reactive crystallization process based on ATR-FTIR and Raman spectroscopy. *J Chemom*. 2008;22:644–652.
2. Braatz RD. Advanced control of crystallization processes. *Annu Rev Control*. 2002;26:87–99.
3. Nagy ZK, Chew JW, Fujiwara M, Braatz RD. Comparative performance of concentration and temperature controlled batch crystallizations. *J Process Control*. 2008;18:399–407.
4. Khan S, Mahmud T, Penchev RY, Roberts KJ. Closed loop control of supersaturation using ATR-FTIR spectroscopy in batch cooling crystallization of an organic compound in an industrial pilot-scale crystallizer. In: Jansens JP, Ulrich J, editors. *Seventeenth International Symposium on Industrial Crystallization ISIC17-CGOM8 Proceedings*. Maastricht, 2008;2:19–26.
5. Kee NCS, Tan RBH, Braatz RD. Selective crystallization of metastable a-form of L-Glutamic acid through feedback concentration control. *Cryst Growth Des*. 2009;9:3044–3051.
6. Schöll J, Vicum L, Muller M, Mazzotti M. Precipitation of L-glutamic acid: determination of nucleation kinetics. *Chem Eng Technol*. 2006;29:257–264.
7. Abebe SB, Wang XZ, Li R, Roberts KJ, Lai X. The information content in NIR spectral data for slurries of organic crystals. *Powder Technol*. 2008;179:176–183.
8. Dunuwila DD, Carroll LB, Berglund KA. An investigation of the applicability of attenuated total reflection infrared spectroscopy for measurement of solubility and supersaturation of aqueous citric acid solutions. *J Cryst Growth*. 1994;137:561–568.
9. Qu H, Alatalo H, Hatakka H, Kohonen J, Louhi-Kultanen M, Reinikainen SP, Kallas J. Raman and ATR FTIR spectroscopy in reactive crystallization: simultaneous monitoring of solute concentration and polymorphic state of the crystals. *J Cryst Growth*. 2009;311:3466–3475.
10. Hirokawa S. A new modification of L-glutamic acid and its crystal structure. *Acta Crystallogr*. 1955;8:637.
11. Higuchi T. *Biochemistry and Molecular Biology of Wood*. New York: Springer, 1997.
12. Robert K, Murray RK, Granner DK, Mayes PA, Rodwell VW. *Harpers's Biochemistry*, *23rd ed*. New Jersey: Appleton & Lange, 1993.
13. Aro A, Mutanen M, Uusitupa M. *Ravitsemustiede*. Helsinki: Duodecim, 2005.
14. Rovner SL. Molecules for memory. *Chem Eng News*. 2007;85:22–24.
15. Black SN, Davey RJ, Halcrow M. The kinetics of crystal growth in the presence of tailor-made additives. *J Cryst Growth*. 1986;79:765.
16. Nývlt J, Ulrich J. *Admixtures in Crystallization*. Weinheim: VCH Verlagsgesellshaft, 1995.
17. Borissova A, Jammoal Y, Javed KH, Lai X, Mahmud T, Penchev R, Roberts KJ. Modeling the precipitation of L-glutamic acid via acidification of monosodium glutamate. *Cryst Growth Des*. 2005;5:845–854.
18. Partanen JI, Juusola PM, Minkkinen PO. Redetermination of the thermodynamic values of the first and second dissociation constants of glutamic acid in solutions at 29815K. *Acta Chem Scand*. 1998;52:198–206.
19. Pitzer KS, Rabindra NR, Silvester LF. Thermodynamics of electrolytes 7 sulfuric acid. *J Am Chem Soc*. 1977;20:4930–4936.
20. Kirk-Othmer. *Encyclopedia of Chemical Technology*, *3rd ed*. Berlin: Springer, 1984;2:413.
21. Hirayama N, Shirahata K, Ohashi Y, Sasada Y. Structure of α-form of L-glutamic acid. α-*β* transition. *Bull Chem Soc Jpn*. 1980;53:30–35.
22. Lehmann MS, Nunes AC. A short hydrogen bond between near identical carboxyl groups in the α modification of L-glutamic acid. *Acta Crystallogr Sect B: Struct Sci*. 1980;B36:1621.
23. Ono T, ter Horst JH, Jansens PJ. Quantitative measurement of the polymorphic transformation of L-glutamic acid using in situ Raman spectroscopy. *Cryst Growth Des*. 2004;4:465.
24. Grant DJW. Theory and origin of polymorphism. In: Brittain HG, editor. *Polymorphism in Pharmaceutical Solids, Drugs and the Pharmaceutical Sciences*. New York: Marcel Decker, 1999;95:7.
25. Kitamura M, Ishizu T. Growth kinetics and morphological change of polymorphs of L-glutamic acid. *J Cryst Growth*. 2000;209:138–145.
26. Dhamelincourt P, Ramirez FJ. Polarized micro-raman and Fourier transform infrared spectra of L-glutamic acid. *J Raman Spectrosc*. 1991;22:582.
27. Gerson AR, Roberts KJ, Sherwood JN. An instrument for the examination of nucleation from solution and its application to the study of precipitation from diesel fuels and solutions of n-alkanes. *Powder Technol*. 1991;65:243–249.
28. Li RF, Penchev R, Ramachandran V, Roberts KJ, Wang XZ, Tweedie RJ, Prior A. Particle shape characterization via image analysis: from laboratory studies to in-process measurements using an in situ particle viewer system. *Org Process Res Dev*. 2008;12:837–849.
29. Yu ZQ, Chew JW, Chow PS, Tan RBH. Recent advances in crystallization control an industrial perspective. *Chem Eng Res Des*. 2007;85(A7):893–905.
30. Lewiner F, Klein JP, Puel F, Fevotte G. Online ATR-FTIR measurement of supersaturation during solution crystallization processes calibration and application on three solute/solvent systems. *Chem Eng Sci*. 2001;56:2069–2084.
31. Grön H, Borissova A, Roberts KJ. In-process ATR-FTIR spectroscopy for closed-loop supersaturation control of a batch crystallizer producing monosodium glutamate crystals of defined size. *Ind Eng Chem Res*. 2003;42:198–206.

Manuscript received May 13, 2009, and revision received Oct. 9, 2009.